X-RAY STUDY OF THE NEW CHARGE-DENSITY-WAVE PHASE IN 1T-TaS$_2$

SATOSHI TANDA* and TAKASHI SAMBONGI

Department of Physics, Hokkaido University, Sapporo 060 (Japan)

Abstract

Positions of both the first- and second-order satellite reflections in the newly found charge-density-wave phase of 1T-TaS$_2$ are measured by x-ray diffraction. The discommensuration network with a lower symmetry and its stacking sequence are determined. This phase appears on cooling from the nearly-commensurate phase as well as on heating from the commensurate phase, in contrast with results of previous measurements.

1. Introduction

In 1T-TaS$_2$, one of the layered transition-metal dichalcogenides, three charge-density-wave (CDW) phases have been observed [1, 2]. The CDW in the incommensurate (IC) phase above 350 K is characterized by three wave vectors, 120° apart from each other, $\vec{q}_i = 0.283\vec{G}_i$ where the $\vec{G}_i$s are the shortest reciprocal lattice vectors ($\vec{a}^*, -\vec{b}^*, \vec{b}^* - \vec{a}^*$). As a result, the CDW forms a triangular lattice within the layer. The stacking period perpendicular to the layer is 3c, where c is the spacing of the host lattice layer; the electrostatic interaction between the charge density triangular lattice is believed to be minimized in the fcc-like stacking. In the nearly-commensurate (NC) phase, between ~350 K and 200 K, the trigonal symmetry is still found in the $\{\vec{q}_i\}$, but they rotate by $\varphi \sim 12°$ from the $\vec{G}_i$s and $|\vec{q}_i| = 0.285a^*$ is a little larger than that in the IC phase. Because reflection intensities of the higher order satellites are relatively large, the lattice distortion is not sinusoidal in space, but the commensurate domains form a lattice with the honeycomb network of discommensurations (DC). The detailed structure of the DC network and the stacking sequence have been studied theoretically by Nakanishi and Shiba [3].

The transition to the commensurate (C) phase at ~200 K is of first order; both $|\vec{q}_i|$ and φ change discontinuously. In the C-phase $\varphi = 13.9°$ and

---

*Present address: Research Center, Komatsu Ltd., Shinomiya, Hiratsuka 254 (Japan)

$|\vec{q}_i| = 0.277a^*$. The commensurability is satisfied by the relation $3\vec{q}_i - \vec{q}_j = \vec{G}_k$. In a previous paper [4] we reported that, while the C-CDW structure is developed within each layer, x-ray satellite reflections are broad along the c^* direction; the stacking of the C-CDW layers is disordered. Nakanishi and Shiba [5] succeeded in analysing the lineshape of super-lattice reflections. Their result is that the stacking is realized by an alternate repeat of the stacking vector c and $2a + c$, where $na + c$ means that a layer stacks on the adjacent one with its origin shifted by $n\vec{G}_i + \vec{c}$. The disorder comes from the random orientation of $\vec{G}_i$.

Near 280 K anomalies have been observed, only on heating but not during cooling, in the electrical resistivity [6], the thermoelectric power [6] and the thermal expansion along the c-axis [7]. Changes in the backward scattering rate of high energy ions [8] and a peak in the differential scanning calorimetry [9] are indicative of a phase transition at that temperature. Fung et al. [10] found that below 280 K there exists a new phase and proposed that the stacking period in that phase is $7c$. We observed that the new phase between $\sim$200 K and 280 K is incommensurate and triclinic [4], and is called the T-phase hereafter.

Nakanishi and Shiba [5] extended the Landau–Ginzburg–McMillan approach to elucidate the three dimensional triple-q CDW structure by taking into account the interlayer coupling up to the next nearest neighbour layers. They predicted that the structure of the T-phase is approximately striped. Although this feature of the new phase has been reported briefly [4], its details together with the experimental procedure are described here because this is the first observation of the triclinic honeycomb DC lattice. Results of a supplementary experiment on the C-phase are also included.

Before experimental results are presented, possible types of CDW domain configuration are classified, though not comprehensively, because considering their presence is indispensable in analysing the experimental data. The width of the x-ray beam is possibly large compared with the size of an individual domain, so reflection profiles do not always give the internal structure of a single domain but correspond to an ensemble of several types of domains.

(i) α- and β-domains

In both NC- and C-phases and also in the T-phase presented in the later section, the CDW wave vectors are not parallel to the shortest reciprocal vectors, $\vec{G}_i$, but rotate clockwise or anticlockwise. Existence of these two types of rotational degrees of freedom was first observed by Wilson et al. [1] in the C-phase of 1T-TaSe$_2$.

The domain in which wave vectors rotate anticlockwise has been called the α-domain and clockwise the β-domain.

(ii) In-layer 120° domains

In the striped phase of 2H-TaSe$_2$ [11], which appears on heating from the C-phase, the trigonal symmetry is broken. One out of three wave vectors

remains unchanged at the transition, but the other two shrink by ~20% and rotate in opposite directions. Therefore, three kinds of domain are possible with the direction of the commensurate wave vector ±120° apart from each other. In real space the stripe DCs run parallel to each other within a domain but ±120° away from that in the neighbouring domains. In other structures with broken trigonal symmetry, three kinds of in-layer 120° domains are also possible as long as the host lattice has trigonal symmetry.

(iii) Possible types of domain arising from the stacking sequence

As long as the triple-q CDWs are developed, they form the trigonal lattice of charge density within each layer. The electrostatic interaction between layers of point charges is minimized by the fcc-like stacking. For example, in the C-phase of 1T-TaSe$_2$ the stacking sequence of the super-lattice layers is specified by the stacking vector $2a + c$; the layers are stacked successively with the equivalent positions of the next layer displaced by $2\vec{L}_i + c$, where $\vec{L}_i$ is one of the shortest lattice vectors $\vec{a}$, $\vec{b}$ and $-(\vec{a} + \vec{b})$ (specified as σ_{ci} by [5]). Therefore, there can exist three types of domain with different $\vec{L}_i$s. Larger variety comes from the operation $\vec{L}_i \rightarrow -\vec{L}_i$ (speci-fied as $\bar{\sigma}_{ci}$ by [5]). In the IC-phase of 1T-TaS$_2$ the two types, σ_{ci} and $\bar{\sigma}_{ci}$, are distinguished by the c^*-positions of the first-order satellite at ±1/3. If both —ABCABC— and —ACBACB— sequences are possible in both α- and β-domains, there will appear two reflections in a scan along the c^*-axis, at +1/3 and −1/3. On the other hand, if the choice of α- or β-domain is coupled with the stacking sequence as screw, there will appear only one reflection at +1/3 or −1/3.

2. Experimental procedure

Single crystals used in this work were selected from three stocks prepared by T. Tani, with $\rho_\parallel(4.5K) = 2 \times 10^{-2}$, 6.8×10^{-2} and 8.8 Ω cm. A few crystals supplied by R. Inada at ISSP were also used for comparison. As is well known, the transport properties of 1T-TaS$_2$ at low temperature are strongly dependent on the growth conditions. For example, the electrical resistivity within the layer $\rho_\parallel$ below ~100 K is much larger for crystals grown at relatively low temperature (~750 °C) in an atmosphere with excess sulphur compared with crystals grown at 900 ~ 950 °C without excess sulphur. Since anomalous properties at low temperature have been attributed to the Anderson localization, some disorder in the crystal may be found by, *e.g.*, diffraction experiments. This is the reason why we used various samples of different $\rho_\parallel(4.5K)$. The results reported in this paper are, however, essen-tially common to all samples used; no systematic variation beyond experi-mental uncertainty has been found. Moreover, the results are quite repro-ducible; no change was observed after thermal cycling between room temper-ature and 100 K.

Crystals that were flat and relatively thin were selected for the measure-ments. Most crystals in stock were not flat but slightly curved. They were
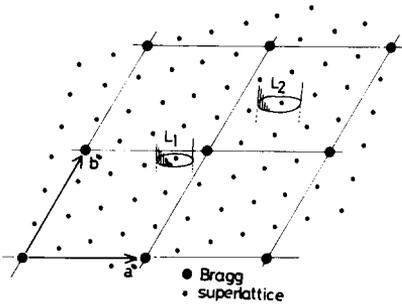
Fig. 1. Reciprocal lattice. The satellite reflections near L_1 and L_2 are used to determine the wave vectors.

discarded because they show broad reflection peaks along the c^*-axis. The sample was fixed by Apiezen N grease to a sample holder with the c^*-axis perpendicular to the ω-axis. Reflection intensity was measured within the regions of the reciprocal lattice shown in Fig. 1. The first- and second-order satellite/super-lattice reflections are observed near L_1 and L_2, respectively. These regions were selected for experimental convenience; they are near the $(1, 1, 0)$ plane. The positions of satellite reflections can be determined accurately by referring to those of the Bragg $(1, 1, l)$ reflections. Details of the x-ray apparatus used in this work are described in ref. 12.

3. C-phase

Although diffraction profiles in the C-phase have been reported in our previous paper [4], measurements were repeated with different samples to examine whether the profile, especially its width, is dependent on $\rho_\parallel(4.5K)$.

Because it has been established by electron and x-ray experiments [1, 2] that the in-layer positions of the super-lattice reflections* are $(10/13)a^* + (12/13)b^*$ near L_1 and $(18/13)a^* + (19/13)b^*$ near L_2, we are solely concerned with their c^* positions.

The profile† at 150 K along $(10/13, 12/13, \zeta)$ is shown in Fig. 2 for a sample of $\rho_\parallel(T = 4.5 \text{ K}) = 8.8 \ \Omega$ cm and in Fig. 3 for $\rho_\parallel(T = 4.5 \text{ K}) = 2.0 \times 10^{-2} \ \Omega$ cm. No difference is found between the two samples; the difference in $\rho_\parallel(T = 4.5 \text{ K})$, an indication of the degree of disorder which results in the Anderson localization, has no effect on the diffraction profile.

---

*To examine the reliability of our results, the distance $|q|$ between $(1, 1, 0)$ and $(10/13, 12/13, 0)$ was measured by assuming the angle between $\vec{q}_1$ and $\vec{a}^*$ is $13.9°$. The obtained value $|q| = (0.277 \pm 0.001)a^*$ is in good agreement with $|q| = (1/\sqrt{13})a^* = 0.27735a^*$ required by the commensurability.

†These satellites are of the α-domain. The β-satellites are observed by rotating the sample around the χ-axis, which is perpendicular to both ω- and c^*-axes, by $\sim 3°$.
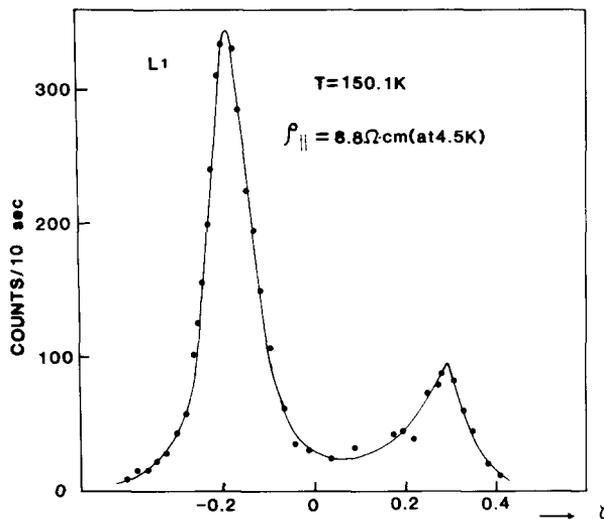
Fig. 2. Profiles of super-lattice reflections in the commensurate phase, at 150 K, near L_1 for a sample with the high electrical resistivity at ~ 4 K.
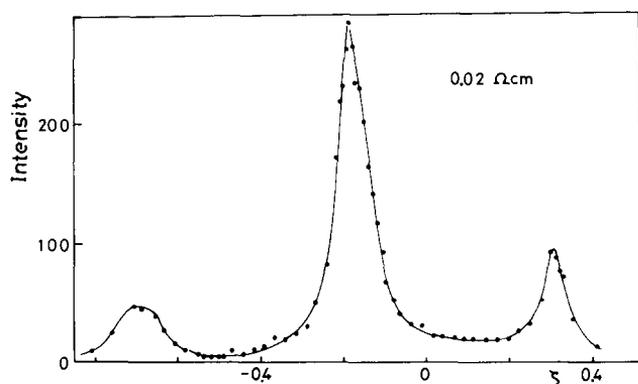

Fig. 3. Profiles of super-lattice reflections in the commensurate phase, at 150 K, near L_1 for a low-resistivity sample.

Important features of the C-phase are:

(1) along $(10/13, 12/13, \zeta)$ two broad peaks appear at $\zeta = (0.310 \pm 0.003)c^*$ and $(0.825 \pm 0.003)c^*$ and the intensity of the latter is about four times as large as the former;

(2) along $(18/13, 19/13, \zeta)$ a peak appears at $\zeta = (0.020 \pm 0.003)c^*$ with a width larger than that near L_1;

(3) everywhere on both lines $(10/13, 19/13, \zeta)$ and $(18/13, 19/13, \zeta)$ the intensity is larger than the background;

(4) the broadness is common to all samples examined and independent of the cooling rate from room temperature and of thermal cycling. Between ~ 100 K and 200 K the profile is independent of temperature.

The broadness of the superlattice reflections is intrinsic because the width of the Bragg reflection $(1, 1, 0)$ is $\sim 0.001c^*$ in the C-phase as well as in the NC-phase; the stacking of the CDW layers is disordered in spite of the good quality of the crystal.

We assume that the stacking sequence of the CDW layers can be specified by assigning a single stacking vector,

$$\vec{S} = x\vec{a} + y\vec{b} + \vec{c} \equiv \vec{U} + \vec{c}. \tag{1}$$

The structure factor is then given by

$$F(\vec{K}) = \sum_{p}^{\text{layer}} \sum_{i} \exp\left\{2\pi i \vec{K} \cdot \left[\vec{r}_i + \sum_{j=1}^{3} \vec{A}_j \sin(2\pi \vec{q}_j \cdot (\vec{r}_i - p\vec{U}))\right]\right\}$$

where the CDW pattern is displaced by $p\vec{U}$ in the pth layer. Satellite reflections appear at

$$\vec{K} = (h\vec{a}^* + k\vec{b}^* + l\vec{c}^*) + (\alpha\vec{q}_1 + \beta\vec{q}_2 + \gamma\vec{q}_3) - \{(\alpha\vec{q}_1 + \beta\vec{q}_2 + \gamma\vec{q}_3) \cdot \vec{U}\}\vec{c} \tag{2}$$

where α, β, γ are integers.

In the C-phase, only $\vec{U} = n\vec{G}_i$ with $n = 0, 1, 2$ is possible. If $n = 1$ as proposed by Scruby et al. [2], reflections would appear near L_1 at $\zeta = -(1/13)c^*$, $-(3/13)c^*$ and $(4/13)c^*$ and near L_2 at $\zeta = (2/13)c^*$, $(5/13)c^*$ and $(6/13)c^*$ because of the three kinds of in-layer $120°$ domain.

Similarly, neither the case $n = 0$ nor $n = 2$ is what is observed. Nakanishi and Shiba succeeded in reproducing our experimental results as fully discussed in [5]. In their model, every two adjacent layers are coupled by $\vec{S} = \vec{c}$ and the pair is stacked by $\vec{U} = 2\vec{G}_i$, but the direction of $\vec{G}_i$ is completely random. The agreement with the observed profiles is demonstrated in Fig. 8 of their paper [5].

4. Intermediate phase (T-phase)

On heating the sample from below 200 K, the super-lattice reflections disappear at ~ 220 K and three sharp new reflections are observed near L_1 and another three near L_2. These reflections are hereafter called T-satellites. Near 280 K these T-satellites disappear and the NC-satellites are recovered. This transition has been detected as anomalies of various properties [6 - 9]. Between 220 K and 280 K only the T-satellites are observable but not the NC-satellite nor the C-super-lattice reflection, even after thermal cycling, in all samples examined (irrespective of the resistivity at ~ 4 K). The T-satellites are sharp; widths are of the same order of those of Bragg reflections along the c^*-direction as well as parallel to the a^*-b^* plane. After keeping the sample at 150 K for several hours positions of the T-satellites were measured with reference to the positions of Bragg $(1, 1, 0)$ and $(1, 1, 1)$. The results are summarized in Table 1.

TABLE 1

In-layer wave vectors (absolute magnitude $|\vec{Q}_i|$ and its angle φ from $\vec{G}_i$) in the T-phase and ζ, the c^*-position of the T-satellites

	225 K			270 K		
	Q/a^*	φ (°)	ζ/c^* (± 0.001)	Q/a^*	φ (°)	ζ/c^* (± 0.001)
Q_1	0.286	15.8	0.439	0.288	15.6	0.434
Q_2	0.299	14.1	0.242	0.303	13.4	0.264
Q_3	0.285	12.62	0.319	0.286	11.84	0.302

Fig. 4. First-order satellite reflections in the T-phase, at 225 K, on heating from the commensurate phase.

Three T-satellites are observed near L_1, as shown in Fig. 4. Their c^*-components (q_{ci}) are incommensurate and $q_{c1} + q_{c2} + q_{c3} = 1.000$ as expected from the relation (3) below and (2). The second-order T-satellites observed near L_2 are shown in Fig. 5. Their c^*-components, -0.184 ± 0.003, $+0.115 \pm 0.003$, $+0.061 \pm 0.003$, are equal to $q_{c2} - q_{c1}$, $q_{c1} - q_{c3}$ and $q_{c3} - q_{c2}$ respectively. Therefore, these three second-order satellites come from three kinds of in-layer 120° domain (of α-orientation). Both the in-layer and the c^*-components show weak temperature dependence, as summarized in Table 1.

In-layer wave vectors $\vec{Q}_i$ were obtained after the procedure explained below. More direct determination was impossible because the rotation angles of the sample around two mutually perpendicular axes (χ and φ), both of which are perpendicular to the ω-axis, were not measured accurately enough. The measured quantities are:

(1) in-layer distances between the first-order T-satellites and the origin of the reciprocal space, l_1, l_2 and l_3;

(2) in-layer distances between the second-order T-satellites and the origin, m_1, m_2 and m_3;

(3) the distance between the Bragg $(1, 1, 0)$ and the origin, L.

The angle between $\vec{Q}_i$ and $\vec{G}_i$ is denoted by θ_i. Using $\theta_1(\theta_2)$ as an adjustable parameter, the magnitude $Q_1(Q_2)$ is calculated from L, $l_1(l_2)$ and $\theta_1(\theta_2)$. Both Q_3 and θ_3 are then calculated using the above Q_1 and Q_2 assuming that the relation

$$\vec{Q}_1 + \vec{Q}_2 + \vec{Q}_3 = 0 \tag{3}$$

holds inside a domain. By comparing l_3 calculated from the above Q_3, θ_3 and L with the measured values, probable values of θ_1 and θ_2 are selected by the restriction that the difference of l_3 must be smaller than $\sim 0.05\%$ (experimental reproducibility). Next, the positions of the second-order satellites are calculated and compared with the measured m_i. The most probable values of the wave vectors are selected by the condition that the positions of all of the second-order satellites must be reproduced within $\sim 0.3\%$, which is the largest scatter of our experimental data.

The most probable $\vec{Q}_i$s are shown in Fig. 6, and in Table 1 together with q_cs. In the Figure, the $\vec{Q}_i$s are numbered clockwise. If they are arranged anticlockwise, the second-order satellites $\vec{Q}_i - \vec{Q}_j$ become degenerate in space in conflict with the experimental finding.

If the incommensurate structure built by the $\vec{Q}_i$s is regarded as the commensurate one but modulated by $\delta\vec{Q}_i = \vec{Q}_i - \vec{Q}_{ci}$, where $\vec{Q}_{ci}$ is the nearest commensurate wave vector, and if the modulation is not uniform but concentrated in space, the discommensuration (DC) network can be constructed using δQ_is. In cases where the $\delta\vec{Q}_i$s are parallel to each other, the phase is striped with parallel DCs arranged periodically. As shown in Fig. 6, the deviations $\delta\vec{Q}_i$ are not parallel to each other. Therefore, the T-phase is not
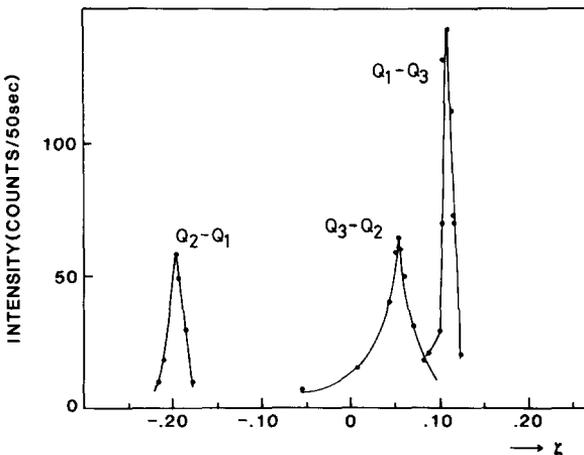

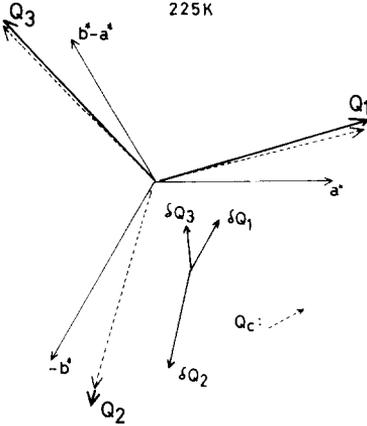Fig. 5. Second-order satellite reflections in the T-phase, at 225 K, on heating from the commensurate phase.

Fig. 6. In-layer wave vectors, $\vec{Q}_i$, of the T-phase at 225 K (thick arrows) and the differences, $\delta\vec{Q}_i$, from the commensurate ones (thin, dotted arrows). The relation between $\delta\vec{Q}_i$s are also shown.

striped but a two-dimensional DC network with broken hexagonal symmetry is developed in this phase.

Because this is the first observation of such a low symmetry DC network, we examine below how the present experimental findings are incompatible with the condition $\delta\vec{Q}_i\|\delta\vec{Q}_j$ within the limits of experimental reliability. First, $\vec{Q}_1$ and $\vec{Q}_2$ are calculated using θ_1 and θ_2 as parameters and the restraint that $\delta\vec{Q}_1\|\delta\vec{Q}_2$ within a domain is used to determine the relation between possible values of θ_1 and θ_2. That restraint is equivalent to the condition that the observed angle between $\delta\vec{Q}_1$ and $\delta\vec{Q}_2$ is $\pm60°$ near L_1 because the observed $\vec{Q}_1$ comes from a kind of in-layer $120°$ domain different from that of $\vec{Q}_2$. Then l_3 and the m_is are calculated as explained above and compared with the experimental values. Figures 7 and 8 show the differences between the calculated and the observed values with θ_1 as the parameter. These differences are larger than allowable for any value of θ_1. For example, if $\theta_1 \gtrsim 16.0°$, the differences of l_3 between the measured and the calculated values are three times as large as the allowable value and two out of three m_is deviate from the measured values by more than 0.4%, which is twice the allowed amount. Thus we conclude that the T-phase is not striped, as long as condition (3) is strictly satisfied.

5. Stretched honeycomb structure of the T-phase

In this section the commensurate domain lattice is constructed from the $\vec{Q}_i$s obtained above. It is assumed that the domain boundary, DC, has the minimum possible phase shift. At 225 K,

$$\vec{Q}_1 = 0.230\vec{a}^* + 0.090\vec{b}^*, \quad \vec{Q}_2 = 0.084\vec{a}^* - 0.332\vec{b}^*. \tag{4}$$
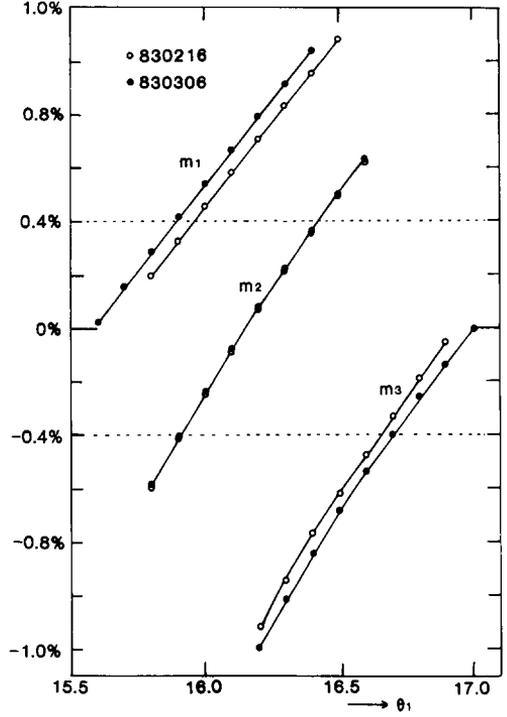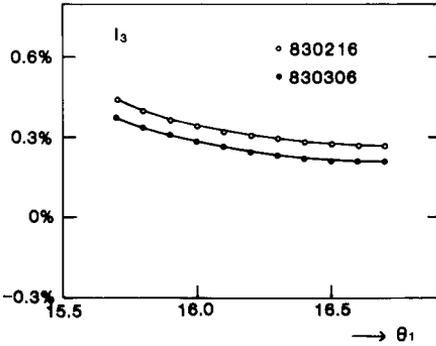
Fig. 7. Difference between the position of the first-order satellite Q_3 assuming the striped structure and that measured in the present experiment.

Fig. 8. Differences between the positions of the second-order satellites assuming the striped structure and the measured ones.

The corresponding translation vectors in real space are

$$\vec{A}_T = 3.95\vec{a} + 1.00\vec{b}, \quad \vec{B}_T = 1.07\vec{a} - 2.74\vec{b}. \tag{5}$$

If the CDW is uniform in space and sinusoidal, $\vec{A}_T$ and $\vec{B}_T$ span the incommensurate triangular lattice. On the other hand, if the modulation is discommensurate, a DC can be found where the distances between the charge density maxima spanned by $(\vec{A}_T, \vec{B}_T)$ and those of the commensurate super-lattice, spanned by

$$\begin{cases} \vec{A}_C = 4\vec{a} + \vec{b} \\ \vec{B}_C = \vec{a} - 3\vec{b} \end{cases} \quad \begin{cases} \vec{Q}_{c1} = (3/13)\vec{a}^* + (1/13)\vec{b}^* \\ \vec{Q}_{c2} = (1/13)\vec{a}^* - (4/13)\vec{b}^*, \end{cases} \tag{6}$$

become $\gtrsim a/2$. To find the domain configuration we temporarily assume that the DC has no width and no surface tension. Starting from the origin of the $(\vec{A}_C, \vec{B}_C)$ lattice, we put the $(\vec{A}_T, \vec{B}_T)$ lattice points on the former. We remain within the same domain as long as

$$|K\delta\vec{A}_T + L\delta\vec{B}_T| < |K\delta\vec{A}_T + L\delta\vec{B}_T + \vec{\Delta}| \tag{7}$$
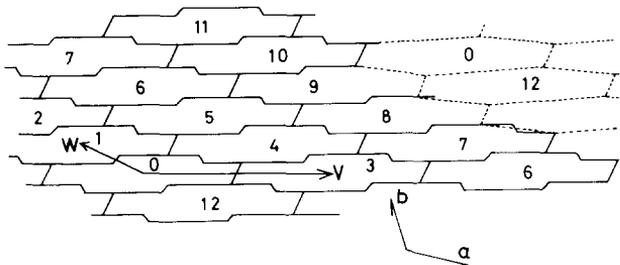
Fig. 9. Domain configuration in the T-phase at 225 K. Full lines show DC constructed assuming that a negligible energy is associated with its length. The dotted lines illustrate an example of probable modifications with reduced DC length.

where $\delta\vec{A}_T = \vec{A}_T - \vec{A}_C$, $\delta\vec{B}_T = \vec{B}_T - \vec{B}_C$, both K and L are integers, and $\vec{\Delta}$ is one of the lattice translation vectors ($|\vec{\Delta}| = a$). If the inequality in (7) is reversed, we have crossed a DC and arrived at one of the neighbouring domains specified by $\vec{\Delta}$, the translation vector of the peak of the C-CDW with respect to the super-lattice.

In Fig. 9, the domain configuration in the T-phase at 225 K is shown. Every domain shows the identical commensurate CDW pattern (and the associated lattice modulation of hexagon star [13]) within it, but the distances between its origin and the super-lattice points increase by $|a|$ as one passes through the domain boundary, DC. The domain lattice has the 3×1 structure as the super-lattice in the C-phase. The domain numbered n is characterized by $\vec{\Delta} = n(-\vec{b})$ (cf. Fig. 1 of [5]). It must be remarked that the configuration constructed as above is commensurate in its strict sense because the vectors connecting the neighbouring domains,

$$\vec{V} = 83\vec{a} + 21\vec{b}, \quad \vec{W} = -24\vec{a} + 6\vec{b} \quad \text{(at 225 K)} \tag{8}$$

are linear combinations of lattice vectors $\vec{a}$ and $\vec{b}$ with integer coefficients. From Fig. 9, the vectors connecting the nearest 0th domains, lattice vectors corresponding to $\delta\vec{Q}_i$, must be equal to $13\vec{W}$, $\vec{V} - 3\vec{W}$, ..., or $n\vec{V} - 3n\vec{W}$ (modulus $13\vec{W}$). From the measured $\vec{Q}_i$ and (6), the lattice vectors reciprocal to $\delta\vec{Q}_1$ and $\delta\vec{Q}_2$ are given as

$$\vec{A} = 303.5\vec{a} + 89.5\vec{b}, \quad \vec{B} = 161.9\vec{a} + 6.7\vec{b} \quad \text{(at 225 K)} \tag{9}$$

Numerical comparison gives the following relations:

$$\vec{A} = 4\vec{V} + \vec{W}, \quad \vec{B} = \vec{V} - 3\vec{W} \tag{10}$$

However, substitution of (8) into (10) gives

$$|\vec{Q}_1| = 0.269, \quad \varphi_1 = 12.08°$$
$$|\vec{Q}_2| = 0.325, \quad \varphi_2 = 12.76°$$

which are different from the measured ones (Table 1) beyond the experimental uncertainty. Therefore, we use the relations (10) but $\vec{V}$ and $\vec{W}$ must be obtained directly from (9) and (10), instead of (8):

$$\vec{V} = 82.5\vec{a} + 21.2\vec{b}, \quad \vec{W} = -26.5\vec{a} + 4.8\vec{b} \tag{8'}$$

which means that a finite fluctuation must be allowed in the domain size.

It must be remembered that the actual shape of a domain is altered to some extent when a finite surface tension is taken into account. For example, if the length of DC is minimized with the nodes of DCs fixed, the domain is hexagonal but distorted, as shown in Fig. 9 by dotted lines. A variety of its variant, hexagonal or tetragonal, can be found with the same size. In any case, the configuration is approximately striped but DCs make a two-dimensional network.

The stacking sequence of the domain lattice layer can be obtained from the measured c^*-components of the T-satellites. The domain layer can be regarded as the commensurate lattice layer modulated by $\delta\vec{Q}_i$. Let the stacking vector be $\vec{U} + \vec{c}$. The in-layer displacement vector $\vec{U}$ is calculated from the relation

$$-\delta\vec{Q}_i \cdot \vec{U} = \zeta_i \tag{2'}$$

where ζ_i is the c^*-position of the satellite $\vec{Q}_i$, or

$$\vec{U} = -(\zeta_1\vec{A} + \zeta_2\vec{B}) \tag{2''}$$

At 225 K, $\vec{U} = -1.998\vec{V} + 0.287\vec{W}$. The corresponding stacking sequence is illustrated in Fig. 10. In this configuration the boundary between the 5th and 6th domains in the first layer is near the centre of the 0th domain in the second layer; $2a + c$ stacking is realized locally (c.f. Fig. 7(a) of [5]). The interaction between DCs is repulsive and long-range interaction cannot be neglected; the W-component of $\vec{U}$ would be approximately equal to 0.5 if only the nearest neighbour interaction is dominant.

As shown in Table 1, both the in-layer wave vectors and the c^*-components are weakly dependent on temperature. The 3×1 stretched honeycomb structure can be found from a similar analysis at 270 K. The T-domain becomes smaller with increasing temperature; the area of a domain at 270 K, $\sim 7 \times 10^3$ Å^2, is smaller than that at 225 K, $\sim 9 \times 10^3$ Å^2. The
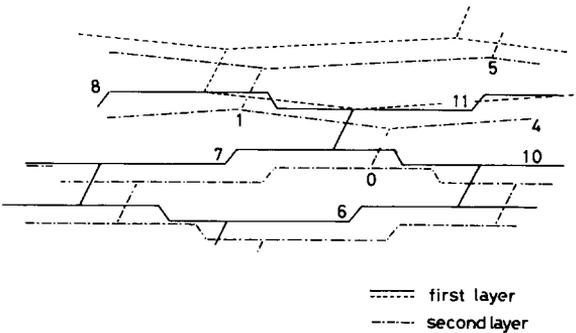

Fig. 10. Stacking sequence of the DC network in the T-phase at 225 K.

former is approximately equal to the area of the NC-honeycomb domain. The stacking vector at 270 K is $-2\vec{V} + 0.358\vec{W}$, where

$$\vec{V} = 70.0\vec{a} + 7.8\vec{b} \quad \text{and} \quad \vec{W} = -16.5\vec{a} + 8.7\vec{b}.$$

6. Observation of the T-phase on cooling

Up to now, the transition to the T-phase has been observed only on heating from the C-phase; no anomaly has been detected in various properties associated with the transition on cooling. However, we found that the T-satellites are observable on cooling below ~250 K. We used four samples, two with $\rho_\parallel(4.5\ \text{K}) = 2.0 \times 10^{-2}$ and the other two with 8.8 Ω cm. In all samples examined, the T-satellites were observed even after thermal cycling down to ~150 K. The experimental findings are summarized below.

(1) On cooling from room temperature, the T-satellites are observed below ~250 K, but the NC-satellites are observed simultaneously. Intensities of the latter are reduced to (1/2) ~ (1/3) compared with those at room temperature and are comparable with the T-satellites.

(2) No temperature dependence of their widths or intensities is detected down to ~200 K. Both types of satellites are sharp, like the NC-satellites at higher temperature. On further cooling, both disappear and only the C-super-lattice reflections are observable.

(3) The satellites observed in a low-resistivity sample are shown in Figs. 11, 12 and 13 and summarized in Table 2. Both α- and β-rotational domains are present, but only Q_1 is observed; the in-layer orientational degree of freedom is lost. Identical results were obtained using another low-
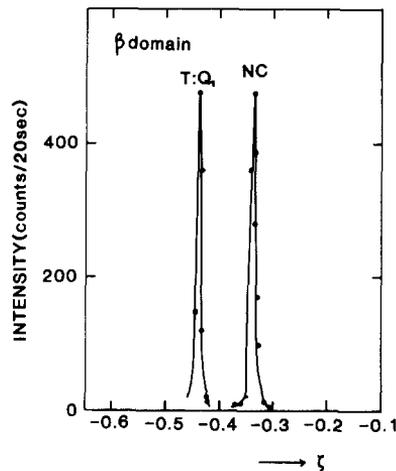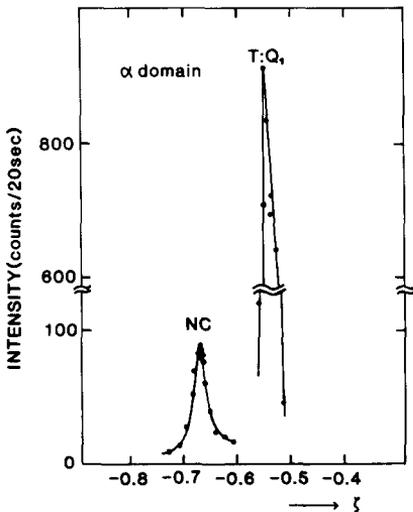

Fig. 11. First-order satellite reflections observed on cooling near L_1 of α-domain.

Fig. 12. First-order satellites observed on cooling of β-domain.
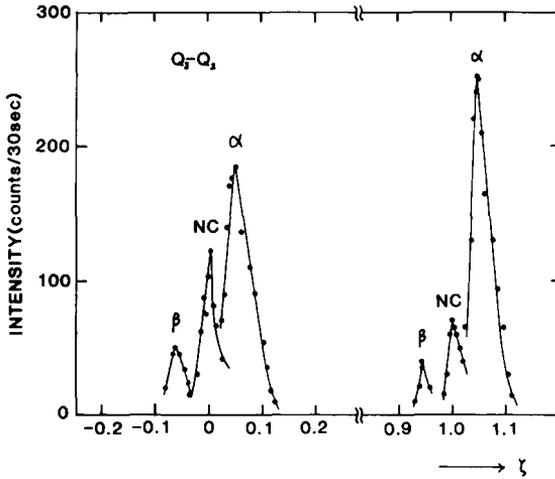
Fig. 13. Second-order satellite reflections on cooling.

TABLE 2

c^*-components of the satellites observed at 230 K on cooling (in units of c^*)

	α		β	
	T-	NC-	T-	NC-
First order	−0.563	−(2/3)	−0.436	−(1/3)
Second order	0.05	0	−0.06	0

resistivity sample and a high-resistivity one. Only in one high-resistivity sample was the T-satellite Q_3, instead of Q_1, observed within the β-domain. The satellites observed near L_2 are the second harmonics of the T- and of the NC-phases; the T- and NC-domains are separated in space.

(4) When the temperature is raised from the coexistence temperature range without further cooling, all the T-satellites vanish at 283 K and the intensities of the NC-satellites increase to the values before cooling.

7. Discussion

The most important problem, why the T-domain is stretched, remains unsolved. In general, the actual domain configuration should be determined taking into consideration the self-energy of DC and the interaction between DCs within the layer as well as on neighbouring layers. Evaluation of these contributions is left for future theoretical studies.

Three problems must be considered.

(1) Appearance of the T-phase on cooling is observed reproducibly in the present work, while no corresponding anomaly has been detected in

various properties. The observed intensities of the T-satellites are not so low, and the intensities of the NC-satellites are halved. Therefore, the total volume of the T-domains must be fairly large, for example, half of the sample size. Moreover, because the T-satellites are sharp, the size of each T-phase region must be large. There is no reason, in principle, why a change in bulk properties cannot be detected as the T-phase appears on cooling.

(2) The T-phase appears on cooling but always in coexistence with the NC-phase. In our experimental arrangement one side of the sample is cemented to a lead holder by Apiezon N grease. Because the sample environment is evacuated and no exchange gas is used, there is an inevitable temperature gradient inside the sample. But the local temperature variation does not exceed ~5 K; the observed transitions are completed within a narrow temperature range and the intensities of the T-satellites do not increase on further cooling. A possible explanation for the incomplete transition is that the NC–T transition is associated with some kind of local distortion and the stress accumulated as a T-phase region grows impedes its further growth.

(3) Only one in-layer 120° domain is observed on cooling, while on heating from the C-phase all three domains are observed. We speculate that the T-domain first appears near the $\alpha-\beta$ boundary and the orientation of the T-domain has a close relation to the direction of the latter. Electron-microscopic observation would be most promising for studying the nucleation/transition kinetics, but it must be mentioned that the a^*-b^* diffraction pattern in the T-phase is quite similar to that in the C-phase.

Some inexplicable phenomena observed during the measurements are mentioned below.

(i) At the NC–C transition, the Bragg reflections were almost completely missing for some minutes. In such a case the intensity was recovered by changing the angle ω (orientation of the sample) by a few degrees. On lowering the temperature by ~5 K, the Bragg peak appeared again at the original position, with the shift of ω less than 0.5°. Far from the transition temperature the Bragg peaks are observable even by rotating the sample by more than 0.5°. A similar phenomenon was observed at the C–T transition. The above observation suggests that at the transitions the crystal suffers temporal macroscopic rotation.

(ii) Just before the NC–C transition the satellite intensity showed strong fluctuation in time even though the temperature was kept constant within 0.1 K. A NC-satellite disappeared for ~10 seconds and appeared repeatedly and another reflection, not yet assigned, was observed near the NC-satellites for seconds. Their appearance or disappearance was aperiodic.

References

1 J. A. Wilson, F. J. DiSalvo and S. Mahajan, *Adv. Phys., 24* (1975) 117.
2 C. B. Scruby, P. M. Williams and G. S. Parry, *Phil. Mag., 31* (1975) 255.
3 K. Nakanishi and H. Shiba, *J. Phys. Soc. Jpn., 43* (1977) 1839.
4 S. Tanda, T. Sambongi, T. Tani and S. Tanaka, *J. Phys. Soc. Jpn., 53* (1984) 476.
5 K. Nakanishi and H. Shiba, *J. Phys. Soc. Jpn., 53* (1984) 1103.
6 T. Tani and S. Tanaka, *J. Phys. Soc. Jpn., 53* (1984) 1790.
7 O. Sezerman, A. M. Simpson and M. H. Jerico, *Solid State Commun., 36* (1980) 737.
8 T. Haga, Y. Abe and Y. Okwamoto, *Phys. Rev. Lett., 51* (1983) 678.
9 S. C. Bayliss, A. M. Ghorayeb and D. R. Guy, *J. Phys. C, 17* (1984) L533.
10 K. K. Fung, J. W. Steeds and J. A. Eades, *Physica, 99B* (1980) 47.
11 R. M. Fleming, D. E. Moncton, D. B. McWhan and F. J. DiSalvo, *Phys. Rev. Lett., 45* (1980) 576.
12 K. Tsutsumi, T. Sambongi and A. Toriumi, *J. Phys. Soc. Jpn., 49* (1980) 837.
13 R. Brouwer and F. Jellinek, *Physica, 99B* (1980) 51.